Contrasting late-glacial paleoceanographic evolution between the upper and lower continental slope of the western South Atlantic

Leticia G. Luz[1], Thiago P. Santos[2], Timothy I. Eglinton[3], Daniel Montluçon[3], Blanca Ausin[3], Negar Haghipour[3], Silvia M. Sousa[4], Renata Nagai[5], Renato S. Carreira[1]

[1]LabMAM/Departamento de Química, Pontifícia Universidade Católica do Rio de Janeiro (PUC-Rio), Rio de Janeiro, Brasil

[2]Programa de Geociências (Geoquímica), Universidade Federal Fluminense, Niterói, Brazil

[3]Department of Earth Science, Geological Institute, ETH Zürich, Zürich, Switzerland

[4]Instituto de Oceanografia, Universidade de São Paulo, São Paulo, Brasil

[5]Centro de Estudos do Mar, Universidade Federal do Paraná (UFPR), Paraná, Brasil

Correspondence to: Leticia G. Luz (leticiagluz@gmail.com)

Abstract. The number of sedimentary records collected along the Brazilian margin has grown significantly in recent years. However, few are useful in elucidating the paleoclimatic evolution of relatively shallow waters (< 1,000 m in depth) influenced by continental shelf areas. In this study, we present traditional and new organic and inorganic proxies (alkenones-derived SST, δD-alkenones, δ^{18}O of planktic foraminifera and ice-volume free seawater δ^{18}O$_{IVF-SW}$) to assess changes in sea surface temperature (SST) and the salinity of two sediment cores (RJ-1501 and RJ-1502) sampled from the subtropical western South Atlantic during the end of the last glacial cycle. Although they are separated by only 40 km, these records present a contradictory climatic evolution through the study period, with the shallower (deeper) core RJ-1501 (RJ-1502) displaying consistently cold (warm) and fresh (salt) conditions toward the Last Glacial Maximum and last deglaciation. We reconciled these results considering that the RJ-1501 site was under the influence of cold and fresh waters transported northward by the Brazilian Coastal Current (BCC), which carried a signal from mid- to high-latitudes temperature and freshwater discharged by the La Plata River to the study area. Comparing the RJ-1502 results with other deeper cores collected from this area support this interpretation. Our data indicate that a steep thermal and density gradient was formed between the BCC and Brazil Current (BC) during the last climate transition, which may have generated perturbations in the air-sea heat flux, with consequences for the regional SE South America climate. In a scenario of future weakening of the Atlantic Meridional Overturning Circulation, the reconstructed gradient may become a prominent feature in the region.

1 Introduction

Paleoclimatic knowledge accessed through marine sediment cores along the Brazilian margin has increased significantly in the last decades (e.g., Arz et al., 1999, 2001; Chiessi et al., 2008; Govin et al., 2014; Jaeschke et al., 2007;

Jennerjahn et al., 2004; Lessa et al., 2017; Mulitza et al., 2017; Portilho-Ramos et al., 2015; Rühlemann et al., 1999). Cores located adjacent to the semi-arid NE Brazil have allowed for several investigations addressing the interplay between changes in the Atlantic Meridional Overturning Circulation (AMOC), the sea surface temperature (SST) of the tropical Atlantic, and the continental climate (in terms of precipitation and vegetation cover) in centennial to millennial time-scales (Behling et al.,

35   2000; Bouimetarhan et al., 2018; Burckel et al., 2015; Crivellari et al., 2019; Venancio et al., 2018; Zhang et al., 2015, 2017). Marine records recovered from the subtropical realm (southern to 20 ºS) generally do not show obvious surface millennial-scale features like those from NE Brazil (Santos et al., 2017a); nonetheless, this area suffers significant changes in wind-driven upwelling patterns, with consequences for regional upper-ocean productivity (Lessa et al., 2019; Portilho-Ramos et al., 2019). The subtropical Brazilian margin may also be a sensitive region to the transmission of the Agulhas rings to the South Atlantic

40   at the end of glacial periods, highlighting its importance for glacial-interglacial transitions (Santos et al., 2017b). Similarly, the application of cores in the subtropical margin is exceptional in exploring changes in the water mass composition of the deep Atlantic during the last glacial cycle (Howe et al., 2018; Lund et al., 2015; Oppo et al., 2015; Tessin and Lund, 2013).

Most of these studies were based on intermediate to deep-water cores (> 1500 m) recovered from the mid- to lower-continental slope, and investigations supported by shallower cores (< 1000 m) are generally limited to the Holocene (e.g.,

45   Albuquerque et al., 2016; Lessa et al., 2016; Nagai et al., 2014). Such a shorter-time range from shallow-water cores is due to the fact that wide regions of the continental shelf were exposed during the last glacial cycle, and that the sea-level rise of the last deglaciation provoked massive sedimentological disturbances, preventing the acquisition of well-organized chronological sequences. This hindrance was partially circumvented by cores GeoB2107-3 and GeoB6211-2, in which dinocyst assemblage reconstructions were developed (Gu et al., 2017; Gu et al., 2018). These authors verified the presence of eutrophic taxa along

50   the SE Brazilian coast from the late glacial to the last deglaciation, assigning this to the high input of continental nutrients carried by the Brazilian Coastal Current (BCC) that flowed farther from the shore, due to the low sea-level. However, a more straightforward hydrographic reconstruction of the eventual influence of the BCC along the southern portion of the Brazilian continental margin is still lacking. This limits the elaboration of detailed knowledge about the regional climatic evolution, mainly for inner parts of the coast that might receive the influence of the BCC.

55   The BCC is a seasonal coastal current flowing northward in the continental shelf from the Argentinean shelf and southern Brazilian shelf that transports a mixture of cold and low-salinity Plata Plume Water (generated by the discharge of the La Plata River) and Subantarctic Shelf Water (derived from the northern extension of the Malvinas Current) (Möller et al., 2008; de Souza and Robinson, 2004). The BCC is forced by the prevailing southern winds allied to the meridional oscillations of the Brazil-Malvinas Confluence, and biota related to their water masses have been identified as far north as 22ºS (near the

60   city of Rio de Janeiro) (Stevenson et al., 1998). The cold and low-salinity BCC exhibits very contrasting hydrographic patterns compared to those of the warm and high-salinity Brazil Current (BC) (Mendonça et al., 2017). As a consequence, the presence of the BCC over the continental shelf produces a strong cross-shelf SST gradient toward the shelf break, where BCC waters meet the opposite flowing of the BC. The gradient imposed by the front may disturb atmospheric properties, such as surface

wind stress, stability, and air-sea flux exchange, as the sea surface in this region can act as a heat source to the atmosphere (Pezzi et al., 2016). Hence, BCC dynamics are a determining climate factor along the SE Brazilian coast.

In terms of climate reconstruction, sediment cores retrieved from areas under the influence of the BCC may not follow temperature and salinity patterns previously reconstructed for the BC (e.g., Santos et al., 2017a). Moreover, the BCC carries a fingerprint of the continental climate, as most of the drainage systems in the SE Brazil flow inland to the Paraná Basin and are discharged to the ocean by the La Plata River. This makes the marine cores under the BCC sedimentation regime ideal in also reconstructing inland climate conditions from the continental runoff in the subtropical western South Atlantic. Herein, we present a paleoceanographic reconstruction based on two sediment cores collected in the upper (RJ-1501, 328 m water depth) and lower (RJ-1502, 1598 m water depth) continental slope using organic (alkenones-derived SST and δD-Alkenones) and inorganic (δ^{18}O of planktic foraminifera and ice-volume free seawater δ^{18}O$_{IVF-SW}$) proxies for the last glacial transition. Our multi-proxy reconstruction indicates that RJ-1502 (the furthest record from the coast) agree relatively well with earlier studies developed in the BC core (Santos et al., 2017a), which reported a gradual build-up in the temperature and salinity along the end of the last glacial towards the Holocene without minimum SST during the Last Glacial Maximum (LGM). On the other hand, the shallower RJ-1501 revealed that the evolution of inner waters occurred in the opposite direction. This core indicates an accentuated cooling around the LGM and an increase in continental freshwater discharge during the last deglaciation. We interpret this antagonism as the result of the influence of the BCC and its cold low-salinity waters that carried (i) the temperature evolution pattern from the mid- to high- South Atlantic latitudes , and (ii) the enhanced precipitation signal in the adjacent SE South America during the last deglaciation to the study area. Our data, therefore, strengthen knowledge on the long-term circulation changes in this region and highlight the nonlinearity of the climate system even in neighbouring regions.

2 Material and Methods

2.1 Sediment cores

Gravity cores RJ-1501 (23°58'14.3" S/43°06'35.1" W, water depth: 328 m, length: 402 cm) and RJ-1502 (24°32'57.6" S/42°55'42.9" W, water depth: 1598 m, length: 250 cm) (Figure 1) were collected from the slope off southeast Brazilian Continental Margin by RV Inspector II in June 2015 (Figure 1). Due to the chronological limitation of ^{14}C dating, only the first 250 cm of the RJ-1502 core were considered in this study. Both cores were sliced at 3 cm intervals, resulting in 134 and 84 samples for cores RJ-1501 and RJ-1502, respectively. Samples were stored frozen in an aluminum container and subsequently freeze-dried.

2.2 Regional settings

The current study was carried out with sediment cores collected from the upper and intermediate slopes of the state of Rio de Janeiro, Santos Basin (Figure 1), located in the subtropical western South Atlantic. The offshore circulation in the area is governed by the western portion of the anticyclonic movement of the South Atlantic Subtropical Gyre. The South Equatorial Current reaches the Brazilian margin and is distributed into two surface flows, at approximately 10-15º S, namely the North Brazil Current and the BC (Peterson and Stramma, 1991; Stramma and England, 1999). The BC flows south along the Brazilian margin with a total width of 400-500 m, carrying the nutrient-poor Tropical Water (TW: T>20°C; S>36) in its upper ~ 100 m and the nutrient-rich South Atlantic Central Water (SACW: T=6-20°C; S~34.6-36) (Silveira et al., 2017) below. At 33-38ºS, the southward flow of the BC meets the northward flow of the Malvinas Current to form the Brazil-Malvinas Confluence. The position of the Brazil-Malvinas Confluence presents a strong seasonality, moving to a lower latitude (~ 34 ºS) with a northward penetration of the Malvinas Current during the austral winter and a higher latitude (~ 40 ºS) with a southward penetration of the BC during the austral summer (Olson et al., 1988). Both the BC and Malvinas Current are deflected eastward at the Brazil-Malvinas Confluence region, feeding the South Atlantic Current.

Over the continental shelf of the subtropical western South Atlantic, water masses are originated by the dilution of open ocean waters from the western boundary currents. Two distinct water masses are identified, the cold and low-salinity Subantarctic Shelf Water and the warm and high-salinity Subtropical Shelf Water (Piola et al., 2008). The origin of the Subantarctic Shelf Water is related to precipitation excess and continental runoff in the southeast Pacific that penetrates the South Atlantic south of Cape Horn, flowing northward. The Subtropical Shelf Water is fed by the detachment of the TW from the surface layer of the BC. At ~ 33 ºS, a narrow frontal zone, referred to as the Subtropical Shelf Front, separates the two water masses (Piola et al., 2000). A cross-shelf section indicates no penetration of the Subantarctic Shelf Water north of Subtropical Shelf Front, yet hydrographic and satellite observations indicate that cold (14-17 ºC) and low-salinity (33.0-34.0) water tongues can be traced to latitudes as low as 23 ºS (Campos et al., 1996). This low-SST and salinity water observed beyond the front is associated with the northward spreading of the La Plata River outflow (Möller et al., 2008). The discharge of the so-called Plata Plume Water produces a major impact on vertical stratification, since northward penetration of the river plume is associated with decreased surface salinity (Palma et al., 2008; Piola et al., 2005). Along the southern Brazilian margin, the northward movements of the Subantarctic Shelf Water and Plata Plume Water are determined by the BCC. The BCC is a wintertime coastal current flowing northward on the continental shelf, forced by the prevailing southern winds of the winter and meridional displacement of the Brazil-Malvinas Confluence (de Souza and Robinson, 2004). The BCC, therefore, carries cold and low-salinity waters northward and flows opposite the BC, which carries warm and salty waters southward. The shearing between these two currents produces an intense across-shore thermal gradient in which mass and heat exchanges occur via turbulent mixing along their boundaries (Mendonça et al., 2017; Pezzi et al., 2016).

2.3 Age model

The RJ-1501 and RJ-1502 core chronologies were obtained through AMS ^{14}C dating over the shells of the surface-
125   dwelling planktic foraminifera *Globigerinoides ruber* and *G. sacculifer*. AMS ^{14}C were measured in ten and eight samples of
cores RJ-1501 and RJ-1502, respectively (Table 1). Each sample comprised roughly 10 cm³ of sediment, and 50 shells of the
mentioned species were handpicked using a stereomicroscope from the 250 µm size-fraction. AMS ^{14}C ages were determined
at the ETH Laboratory of Ion Beam Physics (Zurich) using the mini radiocarbon dating System (MICADAS). This system is
based on a vacuum insulated acceleration unit that uses a commercially available 200 kV power supply to generate acceleration
130   fields in a tandem configuration. This technique is capable of determining low ^{14}C concentrations due to the high energies
employed in the particle accelerator and the magnetic and electrostatic mass analyzers (Synal et al., 2007).

The age-depth model was built using the Bacon v. 2.3 software, which uses Bayesian statistics to reconstruct Bayesian
accumulation histories for sedimentary deposits (Blaauw and Christeny, 2011). The ^{14}C ages were calibrated using the IntCal13
curve (Reimer et al., 2013) and modeled with a reservoir age of 375 ± 36 years from ten local records (Figure 2). BACON was
135   run with default parameter settings, except for a higher memory (mem.mean = 0.7) to more consistently define that the
accumulation rate of a particular depth in the cores depends on the depth above it. Ages were modeled using a student-t
distribution, with 33 degrees of freedom (t.a=33, t.b=34) and 10,000 age-depth realizations to estimate median age and 95%
confidence intervals at 3 cm resolutions for each core. Mean 95% confidence ranges were of 2588 and 3861 years for cores
RJ-1501 and RJ-1502, respectively. One hundred percent of the dates lie within the age-depth model in a 95% range for both
140   cores. According to our age-depth models, cores RJ-1501 and RJ-1502 cover the last 42.44 and 53.57 ka BP (Figure 2). The
mean accumulation rate of core RJ-1501 was around 100 years/cm between 40 and 20 ka BP, with a steep increase to 500
years/cm during the last deglaciation and a return to previous values during the Holocene. A general lower accumulation rate
was found for core RJ-1502, with roughly 200 years/cm between 50 and 20 ka and almost 1000 years/cm during the last
deglaciation and Holocene (Figure 2).

145   ## 2.4 Alkenone analyses and sea surface temperature reconstruction ($U_{37}^{K'}$-derived SST)

A total of 139 sediment samples were selected for alkenone analyses, considering the two collected cores. Samples
were freeze dried and homogenized with a mortar and pestle. An 15-30 gram (± 0.1 mg) aliquot of the homogenized material
was extracted in a pressurized solvent extractor system (Dionex® ASE-200) using a mixture of dichloromethane (DCM):
methanol 9:1 (v/v) at 100 °C and 1000 psi in two cycles, 11 minutes per cycle. Before extractions, a known amount of 2-
150   nonadecanone was added as a surrogate standard. The total lipid extracts were saponified (1M KOH at 110 °C for 2h), and the
neutral fraction recovered with *n*-hexane. The neutrals were further fractionated using a Pasteur pipette containing 4 cm of
activated silica into three fractions: apolar (4 mL of *n*-hexane), ketones (4 mL of *n*-hexane:DCM, 2:1/v:v) and polar (4 mL of
DCM:methanol, 1:1/v:v). The alkenones in the ketones fraction were identified and quantified using a Thermo® Focus gas
chromatograph equipped with an Agilent DB-5 capillary column (60 m x 250 µm diameter x 0.25 µm internal film) and a

155   flame ionization detector. The oven temperature program used started at 50 °C, followed by a 20 °C min^{-1} ramp up to 80 °C

and a second ramp at 8 °C min^{-1} up to 320 °C, with a final hold at this temperature for 33 min. The extracts (1 µL) were injected

in spitless mode and He was using as the carrier gas at 1.2 mL min^{-1}. Alkenone identification was based on the retention time

of authentic standards, whereas quantification followed the   internal standard method using n-C$_{36}$ alkane. Analytical precision

was estimated as 12% or better, based on triplicate analyses of a sediment sample. The $U_{37}^{K'}$ values were calculated according

160   to Prahl and Wakeham (1987): $U_{37}^{K'} = C_{37:2}/(C_{37:2} + C_{37:3})$ and were then converted to sea surface temperature ($U_{37}^{K'}$-derived

SST) using the Müller et al. (1998) calibration, as follows: $U_{37}^{K'} = 0.033\ U_{37}^{K'}$-derived SST (^{o}C) + 0,069; r^2 = 0.98; n = 149; DP=

± 1.0 °C.

2.5 Planktic foraminifera oxygen isotope composition (δ^{18}O) of

        The planktic foraminifera species *Globigerinoides ruber* [white] is considered as one of the most reliable indicators

165   for environmental reconstructions in tropical and subtropical latitudes, as it inhabits the mixed layer, its foreheads are formed

(calcified) up to 25 m from the water column and its carapace calcifies within an isotopic oxygen balance with sea water

(Lisiecki and Raymo, 2005). The isotopic oxygen composition (δ^{18}O) was determined in *G. ruber* [white] specimen shells

shells from selected slices of the RJ-1501 and RJ-1502 cores. Approximately 10 mL of sediment were sifted sequentially using

two sieves (63 µm and 150 µm meshes), hand-picking the specimens . Approximately 10-15 shells >150 µm from each sample

170   were weighed in appropriate glass vials to be injected into an automatic Kiel IV Thermo Fisher Scientific® system (automatic

CO$_2$ obtainment device from the analyzed carbonate) for the oxygen isotope analyses. The determination of low ^{18}O isotope

contributions is performed by using the respective ratios with their most abundant elements in the sample. The data were

reported by the delta notation in parts per thousand and relative to the standard Vienna Pee-Dee Belemnite (VPDB). The Kiel

IV carbonate device was coupled to a Thermo Fisher Scientific® Delta V Plus mass spectrometer. The carbonate generated by

175   the forams shells was vacuum dissolved by applying a phosphoric acid 103% drip at a temperature of 70°C and directed to

the mass spectrometer. The masses were calibrated with the international MS2 (δ^{18}O$_{VPDB}$ = 1.81‰, n = 14) and ISOLAB B

(δ^{18}O$_{VPDB}$ = -18.59‰, n = 4) standards and all results were reported as the conventional delta notation in relation to the VPDB

standard. The standard deviations were δ^{18}O = 0.061 for the MS2 standard and δ^{18}O = 0.076 for the ISOLAB B standard.

2.6 Ocean surface salinity tracers (Alkenone hydrogen isotope and Ice-volume free seawater oxygen isotope)

180   The hydrogen isotopic composition of the C$_{37:2-3}$ alkenones (δD-Alkenones) produced by haptophyte algae was used as

a proxy for changes in sea surface salinity (SSS). The F2 fraction separated from the organic lipid extract (see item 2.4) was

used to determine δD-Alkenones by gas chromatography-isotopic ratio mass spectrometry (GC-IRMS; Delta^{plus}XP). A

relatively large volume of each sample (1 to 8 µL, corresponding to a 200-300 ng load of the analyte) was injected using the

system vent mode into an Agilent VF-1ms (60 m x 0.25 mm x 0.5 µm) capillary column. The following oven temperature

185   program was used: initial temperature set at 50ºC for 1 min, heating at 40ºC for 1 min up to 300ºC and then to 320ºC at a rate

of 20ºC min[1], with a final hold of 5 min. He was used as carrier gas. Quantification was based on the external standard method,

using n-C_{27} alkane (Arna Schimmelmann Biogeochemistry Laboratory - University of Indiana). The D/H ratio was quantified

and calibrated through a co-injection with the Vienna Standard Mean Ocean Water (VSMOW) as reference standard, where

δD-Alkenone values are reported as ‰ relative to this reference standard. The samples were injected in duplicate and the

190   acceptable standard deviations were ≤2‰.

        SSS was also evaluated considering the seawater isotope (δ¹⁸O$_{sw}$) and the stable oxygen isotope data for the *G. ruber*

planktic foraminifera shells (δ¹⁸O$_{G\ ruber}$). To determine the sea water oxygen isotope (δ¹⁸O$_{sw}$), *G. ruber* δ¹⁸O values used and

sea surface temperature values were reconstructed from the alkenones ($U^{K'}_{37}$-derived SST) applied in the following equation: *T*

($U^{K'}_{37}$-derived SST) = -4.44 * (δ¹⁸O$_{G ruber}$ - δ¹⁸O$_{sw}$) + 14.20, as proposed by Mulitza et al. (2003). A factor of 0.27‰ was used to

195   convert oxygen-isotope values from VPDB to VSMOW, in order to correctly account for ice volume, based on data reported

by Grant et al. (2012).

3 Results

        As a general result, the same trend was noted for δ¹⁸O, paleotemperature and paleosalinity proxies over the length of

cores RJ-1501 and RJ-1502 (Figure 3A-D). Both records indicate similarity throughout the MIS3 and MIS1 periods. Regarding

200   slope variations (RJ1501 → RJ1502), δ¹⁸O and $U^{K'}_{37}$-derived SST profiles are in agreement throughout the glacial period until

Termination I, when a decoupling occurs and the RJ-1501 data display lower temperature results. From the beginning of MIS

2, a discrepancy between the records indicates a genuine change in behaviour by the main environmental conditions. *G. ruber*

δ¹⁸O values [white and pink] (δ¹⁸O$_{G ruber}$) ranged from -0.97‰ to 0.72‰ (n = 101) in RJ-1501 and from -0.84‰ to 0.95‰ (n

= 72) in RJ-1502 (Figure 3A). A well-defined decreasing trend is observed after the start of the LGM at RJ-1501 that is less

205   clear at the deeper core (RJ-1502). The mean $U^{K'}_{37}$-derived SST for RJ-1501 was 21.8 (± 2.5 °C, n = 77) and more homogeneous

(20.7 ± 1.7 °C, n = 70) for RJ-1502 (Figure 3B). $U^{K'}_{37}$-derived SST varied by 8.2 °C (17.6-25.8 °C) at the location closest to the

shelf break and by 8.9 °C (16.9-25.8 °C) at the slope, with common positive bias at points located at ca. 39 ka and from ca. 12

ka until recenlyt. Nevertheless, the current annual SST means are higher between +0.74 °C (RJ-1501) and +1.19ºC (RJ-1502)

(data from World Ocean Atlas 2013 - WOA13, Locarnini et al., 2013) compared to our data on Holocene sea surface

210   temperature (RJ-1501 = 24.6 ± 0.88 °C and RJ-1502 = 24.8 ± 0.84 °C).

        The paleosalinity interval sampled by the combination of the RJ-1501 and RJ-1502 cores includes the late MIS3 to

MIS1 isotopic stages. Despite the inconsistency of the δ¹⁸O$_{sw}$ and δD-Alkenone patterns between ca. 28 and 25 ka, both

paleosalinity parameters display a high level coherence and a change in the LGM and Last Deglaciation separating the local

conditions of cores RJ-1501 and RJ-1502 is clearly observed (Figure 3C and D). The δ¹⁸O$_{sw}$ records for RJ-1501 and RJ-1502

215   are presented in Figure 3C and reveal a millennial scale variability in the last 50 ka. The mean values of this salinity indicator

were 1.56 (±0.54‰, n = 63) at site RJ-1501 and 1.25 (±0.46‰, n = 95) at RJ-1502. The δD-Alkenone values at RJ-1501 ranged from -181 and -159‰ (n = 47) and between -185 and -153‰ at RJ-1502 (n = 53) (Figure 3D). Decreasing values are observed during the deglaciation and increasing values during the Early Holocene, with high values maintained (~159‰) up to ~ca. 5.5 ka, with a decreasing trend towards the present (up to ca. 1.7 ka).

4 Discussion

The synthesis of global SST carried out by the MARGO project inferred that the subtropical gyres in the Atlantic Ocean experienced very modest cooling (ca. 1 - 2 ºC) in their center during the LGM (Waelbroeck et al., 2009). *G. ruber* Mg/Ca-derived SST from core GL-1090 (collected in the same sedimentary basin as our cores) agree with the MARGO compilation and did not indicate prominent cooling during the LGM (Santos et al., 2017a). Assuming a wider time-scale, the reported temperatures in core GL-1090 during the LGM verified long-term warming developed since ca. 45 ka. According to Santos et al. (2017a), the absence of prominent cooling during the LGM and heat buildup in the region occurred in response to a progressively slower AMOC and glacial climate advance that stored warm waters in the subtropical South Atlantic gyre while sea-ice and ice-caps expanded in southern and northern high latitudes.

We compared the $U_{37}^{K'}$-derived SST from cores RJ-1501 and RJ-1502 to the late-glacial context proposed by Santos et al. (2017a) through core GL-1090. Figures 4A and B show that $U_{37}^{K'}$-derived SST was consistently colder than the Mg/Ca-derived SST throughout the last ca. 50 ka in the area. Despite the obvious deviations in terms of absolute temperature reconstruction that totally different ecology and calibration proxies will display, it is possible to address a similar pattern that emerges between the most offshore RJ-1502 and GL-1090. Both cores recorded progressive temperature increases since the late-glacial towards the Holocene, without significant cooling during the LGM (Figure 4A). This indicates that alkenones and surface-dwelling *G. ruber* were influenced by the BC core , which carried warm waters retained in the South Atlantic subtropical gyre to the Santos Basin during the end of last glacial cycle. Interestingly, $U_{37}^{K'}$-derived SST from RJ-1501 followed an opposite trajectory to that indicated by RJ-1502 and GL-1090 (Figure 4B), where RJ-1501 presented a gradual surface cooling towards the LGM with accentuated warming only after ca. 18.5 ka, despite being separated by only 40 km from RJ-1502. The relative changes in ocean salinity indicated by $\delta^{18}O_{IVF-SW}$ agree with the patterns indicated by the SST reconstructions, i.e., RJ-1502 and GL-1090 cores displayed progressive ocean surface salinification from the late-glacial period to the Holocene (Figure 4C), while RJ-1501 presented surface freshening, achieving its maximum during the LGM and early-deglaciation (Figure 4D). The reconstructed core RJ-1501 parameters were only similar to those from RJ-1502 and GL-1090 during the Holocene (Figure 4). This is strong evidence that the planktic organisms sedimented in RJ-1501 were under the influence of another oceanographic regime during the last glacial cycle.

One could argue that RJ-1501 presented a divergent evolution due to the influence of wind-driven shelf-break SACW upwelling. Although the $U_{37}^{K'}$-derived SST has cooled continuously toward the LGM, temperatures were still warmer than those commonly reported for the occurrence of SACW shoaling (ca. 16 ºC) (Belem et al., 2013). Through the relative abundance of

certain planktic foraminifera species, Lessa et al. (2017) proposed that upwelling in this region from the LGM to the Holocene was rather retracted because the glacial wind-regime (weak NE winds) did not favor the pumping of cold and nutrient-rich

250   deeper waters to the photic zone. Therefore, it is very unlikely that cold SACW tongues accounted for the surface patterns noted for RJ-1501.

Once this alternative explanation is disregarded, it is remarkable that the temperature evolution of core RJ-1501 (with warming only after 18.5 ka) resembles the deglacial pattern inferred from mid- to high-latitudes records for the Southern Hemisphere. $U_{37}^{K'}$-derived SST from ODP Site 1233 (off southern Chile) presented deglacial warming initiated shortly after 19

255   ka (Figure 5A and B). According to the authors, such warming was a combined response of the temperature increase around Antarctica due to the bipolar seesaw during the Heinrich stadial 1 interval and the accentuated release of CO_2 from the deep ocean towards the atmosphere (Lamy et al., 2007) (Figure 5D). Mg/Ca-derived SST from core TNO57-21 (SE South Atlantic) indicated deglacial warming from ca. 18.5 ka, also in response to the pattern imposed by the bipolar seesaw mechanism (Barker et al., 2009). The mean air temperature reconstructed through lipids glycerol dialkyl glycerol tetraethers (GDGTs) from core

260   GeoB6211-2 (SE Brazilian coast) displayed significant warming slightly after the records above (ca. 16.5 ka), but still within the main warming interval in Antarctica (Chiessi et al., 2015) (Figure 5C). Putting these evidence together, such studies suggest that large areas of the northern portion of the Subtropical Front warmed during the early-last deglaciation after the LGM cooling relatively synchronous to Antarctica. It is reasonable to assume that the Malvinas Current could have transported this pattern northward, influencing Subantarctic Shelf Water formation areas. This temperature evolution characterized by a cold

265   LGM can be traced in lower latitudes along the SE Brazilian coast due to the northward-flowing BCC (Figure 5A-E). Apart from the impact of the BCC, cores RJ-1502 and GL-1090 (Santos et al., 2017a) did not record this mid- to high-Southern Hemisphere pattern (Figure 4A).

A recent investigation applying a dinocyst assemblage (core GeoB3202-1, 1090 m water depth) in a region near cores RJ-1501, RJ-1502, and GL-1090 also suggests the occurrence of cold SST during the LGM (Gu et al., 2019). These authors

270   explain the discrepancy between their results and those reported by GL-1090 (Santos et al., 2017a) by invoking shifts in the modern wind-driven upwelling area. Instead, we reason that such conflict could be reconciled by simply considering that shallower cores (RJ-1501, this study and GeoB3202-1, Gu et al., 2019) have a much higher chance of being within the BCC influence zone than deeper records (RJ-1502, this study and GL-1090, Santos et al., 2017a).

During the late-glacial period and Heinrich stadial 1 interval, it is very well documented that large areas in adjacent

275   South America experienced wetter conditions due to a noticeable strengthing of the precipitation associated with the South America Monsoon System (SAMS) (Cruz et al., 2005; Stríkis et al., 2015; Novello et al., 2017; Gu et al., 2018; Stríkis et al., 2018). The increased precipitation volume would be drained by the Parana basin and subsequently discharged into the ocean by the La Plata River, mixing a continental freshwater influence with subantarctic shelf waters, similar to what occurs today (Burone et al., 2013). In this context, BCC waters would carry not only a temperature pattern linked to the thermal evolution

280   of the mid- to high-latitudes of the Southern Hemisphere, but also a sign of low salinity due to higher rainfall throughout the continent. The notion of a fresher surface over the shelf-break area is demonstrated by the $\delta^{18}O_{IVF-SW}$ and δD of RJ-1501 core,

which became progressively lower throughout the late-glacial interval, producing a clear density contrast with the more saline offshore waters (Figure 5F and G). Hence, a stronger BCC influence would explain the residence of colder and fresher surface waters over the RJ-1501 site (and other relatively shallow cores e.g., Gu et al. (2019)), but not in cores collected deeper from
285   the continental slope.

In order to better demonstrate the contrast between the individual cores during the end of the last glacial cycle, we transferred the RJ-1501 age model to RJ-1502 and subtracted the average around zero (RJ-1502 minus RJ-1501) of $U_{37}^{K'}$-derived SST and $\delta^{18}O_{\text{IVF-SW}}$ (i.e., $\Delta\delta U_{37}^{K'}$-derived SST and $\Delta\delta^{18}O_{\text{IVF-SW}}$) (Figure 6). The records were bootstrapped and the 2.5th and 97.5th percentiles are also presented (Figure 6). This exercise demonstrates that a sharp SST gradient was formed toward the
290   LGM and early-deglaciation, reaching a maximum between ca. 20 and 15 ka (Figure 6A). This gradient indicates that the offshore BC waters over the RJ-1502 site were ca. 2 ºC warmer than the inner waters over the RJ-1501 site, which is the double of the annual SST gradient observed today in the region (Figure 1A). In the case of the $\Delta\delta^{18}O_{\text{IVF-SW}}$, the difference achieves ca. 0.8 ‰ in the same period, corresponding to almost a 1.0 salinity unit difference (considering the seawater $\delta^{18}O$-salinity relationship for this region - https://data.giss.nasa.gov/cgi-bin/o18data/). The across-shelf SST gradient caused by the shearing
295   between the BC and BCC is reported as modulating the marine atmospheric boundary layer in the southern Brazilian continental shelf (Mendonça et al., 2017). The atmospheric turbulence caused by heat fluxes from the warm side of the ocean gradient has been investigated as an important factor influencing the weather of coastal regions off southern Brazil (Pezzi et al., 2016). Therefore, our results demonstrate that the background conditions during the end of the last glacial cycle with a disturbed AMOC reduced equatorial heat export and enhanced SAMS (leading to an increase in the La Plata river discharge)
300   created conditions to accentuate the hydrographical contrast between the BC and BCC. Considering the future projections of AMOC weakening (Liu et al., 2017), the gradient strengthening reported herein may be a likely prospect for the southern Brazilian continental shelf.

5 Conclusions

In this study, we reconstructed the SST and $\delta^{18}O_{\text{IVF-SW}}$ through organic and inorganic geochemical proxies from two
305   sediment cores collected from the upper (RJ-1501) and lower (RJ-1502) continental slope of the subtropical western South Atlantic. Although only 40 km apart, these records show considerably distinct hydrographical conditions throughout the end of the last glacial cycle. These contrasting results were reconciled assuming that the shallower and inner RJ-1501 core was under the influence of cold and fresh waters carried by the BCC, while the deeper and more offshore RJ-1502 was under the influence of the warm and saltier BC. A comparison with other records collected in the BC area supports this interpretation.
310   Our results suggest that the conditions experienced during the last glacial transition, i.e., a weak AMOC and strong SAMS, increased the temperature and salinity gradient between the BC and BCC. Depending on the state of AMOC, this scenario may be accentuated in the coming decades.

Code/data availability

The complete dataset can be obtained by requirement to the corresponding author

315 **Author Contributions**

LL, TE and RC conceptualized the study and designed the experiments. LL, DM, BA, NG, SS and RN executed the chemical and/or biological analyses. LL organized all data and prepared the manuscript with contribution from TS and RC. All authors contributed to the manuscript revision, read and approved the submitted version.

Competing interests

320 The authors declare that they have no conflict of interest.

Acknowledgments

We thank Seaseep® for the opportunity of collecting the cores and the R/V Inspector II crew for the support in the field work. We also thank all members of the Laboratory for Ion Beam Physicsat at ETH-Zurich for facilitating the ^{14}C measurements. This study was financed in part by the Coordenação de Aperfeiçoamento de Pessoal de Nível Superior – Brasil (CAPES) – 325 Finance Code 001. Luz thanks CAPES (grant PhD No. 88881.151666/2017-00 and grant PDSE No. 88881.134411/2016-01). R. S. Carreira was supported by research fellowships from CNPq (grant 309347/2017-3)

References

Albuquerque, A. L., Meyers, P., Belem, A. L., Turcq, B., Siffedine, A., Mendoza, U. and Capilla, R.: Mineral and elemental indicators of post-glacial changes in sediment delivery and deposition under a western boundary upwelling system (Cabo Frio, southeastern Brazil), 330 Palaeogeogr. Palaeoclimatol. Palaeoecol., 445, 72–82, doi:https://doi.org/10.1016/j.palaeo.2016.01.006, 2016.

Arz, H. W., Pätzold, J. and Wefer, G.: The deglacial history of the western tropical Atlantic as inferred from high resolution stable isotope records off northeastern Brazil, Earth Planet. Sci. Lett., 167(1–2), 105–117, doi:http://dx.doi.org/10.1016/S0012-821X(99)00025-4, 1999.

Arz, H. W., Gerhardt, S., Pätzold, J. and Röhl, U.: Millennial-scale changes of surface- and deep-water flow in the western tropical Atlantic linked to Northern Hemisphere high-latitude climate during the Holocene, Geology, 29(3), 239, doi:10.1130/0091-335 7613(2001)029<0239:MSCOSA>2.0.CO;2, 2001.

Barker, S., Diz, P., Vautravers, M. J., Pike, J., Knorr, G., Hall, I. R. and Broecker, W. S.: Interhemispheric Atlantic seesaw response during the last deglaciation., Nature, 457(7233), 1097–1102, doi:10.1038/nature07770, 2009.

Bazin, L., Landais, A., Lemieux-Dudon, B., Toyé Mahamadou Kele, H., Veres, D., Parrenin, F., Martinerie, P., Ritz, C., Capron, E., Lipenkov, V., Loutre, M.-F., Raynaud, D., Vinther, B., Svensson, A., Rasmussen, S. O., Severi, M., Blunier, T., Leuenberger, M., Fischer, 340 H., Masson-Delmotte, V., Chappellaz, J. and Wolff, E.: An optimized multi-proxy, multi-site Antarctic ice and gas orbital chronology

(AICC2012): 120-800 ka, Clim. Past, 9(4), 1715–1731, doi:10.5194/cp-9-1715-2013, 2013.

Behling, H., Arz, H. W. and Wefer, G.: Late Quaternary vegetational and climate dynamics in northeastern Brazil , inferences from marine core GeoB 3104-1, Quat. Sci. Rev., 19, 981–994, 2000.

Belem, A. L., Castelao, R. M. and Albuquerque, A. L.: Controls of subsurface temperature variability in a western boundary upwelling

345   system, Geophys. Res. Lett., 40(7), 1362–1366, doi:doi:10.1002/grl.50297, 2013.

Blaauw, M. and Christeny, J. A.: Flexible paleoclimate age-depth models using an autoregressive gamma process, Bayesian Anal., 6(3), 457–474, doi:10.1214/11-BA618, 2011.

Bouimetarhan, I., Chiessi, C. M., González-Arango, C., Dupont, L., Voigt, I., Prange, M. and Zonneveld, K.: Intermittent development of forest corridors in northeastern Brazil during the last deglaciation: Climatic and ecologic evidence, Quat. Sci. Rev., 192, 86–96,

350   doi:10.1016/j.quascirev.2018.05.026, 2018.

Burckel, P., Waelbroeck, C., Gherardi, J. M., Pichat, S., Arz, H., Lippold, J., Dokken, T. and Thil, F.: Atlantic Ocean circulation changes preceded millennial tropical South America rainfall events during the last glacial, Geophys. Res. Lett., 42(2), 411–418, doi:10.1002/2014GL062512, 2015.

Burone, L., Ortega, L., Franco-Fraguas, P., Mahiques, M., García-Rodriguez, F., Venturini, N., Marin, Y., Brugnoli, E., Nagai, R., Muniz,

355   P., Bícego, M., Figueira, R. and Salaroli, A.: A multiproxy study between the Río de la Plata and the adjacent South-western Atlantic inner shelf to assess the sediment footprint of river vs. marineinfluence, Cont. Shelf Res., 55(0), 141–154, doi:http://dx.doi.org/10.1016/j.csr.2013.01.003, 2013.

Campos, E. J. D., Lorenzzetti, J. A., Stevenson, M. R., Stech, J. L. and de Souza, R. B.: Penetration of waters from the Brazil-Malvinas confluence region along the south american continental shelf up to 23°S, Acad. Bras. Ciencias, 68, 49–58, 1996.

360   Chiessi, C. M., Mulitza, S., Paul, A., Pätzold, J., Groeneveld, J. and Wefer, G.: South Atlantic interocean exchange as the trigger for the Bøolling warm event, Geology, 36(12), 919–922, doi:10.1130/G24979A.1, 2008.

Chiessi, C. M., Mulitza, S., Mollenhauer, G., Silva, J. B., Groeneveld, J. and Prange, M.: Thermal evolution of the western South Atlantic and the adjacent continent during Termination 1, Clim. Past, 11(6), 915–929, doi:10.5194/cp-11-915-2015, 2015.

Crivellari, S., Chiessi, C. M., Kuhnert, H., Häggi, C., Mollenhauer, G., Hefter, J., Portilho-Ramos, R., Schefuß, E. and Mulitza, S.: Thermal

365   response of the western tropical Atlantic to slowdown of the Atlantic Meridional Overturning Circulation, Earth Planet. Sci. Lett., 519, 120–129, doi:10.1016/j.epsl.2019.05.006, 2019.

Cruz, F. W., Burns, S. J., Karmann, I., Sharp, W. D., Vuille, M., Cardoso, A. O., Ferrari, J. A., Silva Dias, P. L. and Viana, O.: Insolation-driven changes in atmospheric circulation over the past 116,000 years in subtropical Brazil, Nature, 434(7029), 63–66, doi:10.1038/nature03365, 2005.

370   Epica, C. M.: Eight glacial cycles from an Antarctic ice core, Nature, 429(6992), 623–628, doi:http://www.nature.com/nature/journal/v429/n6992/suppinfo/nature02599_S1.html, 2004.

Govin, A., Chiessi, C. M., Zabel, M., Sawakuchi, A. O., Heslop, D., Hörner, T., Zhang, Y. and Mulitza, S.: Terrigenous input off northern South America driven by changes in Amazonian climate and the North Brazil Current retroflection during the last 250 ka, Clim. Past, 10(2), 843–862, doi:10.5194/cp-10-843-2014, 2014.

375   Grant, K. M., Rohling, E. J., Bar-Matthews, M., Ayalon, A., Medina-Elizalde, M., Ramsey, C. B., Satow, C. and Roberts, A. P.: Rapid coupling between ice volume and polar temperature over the past 150,000 years, Nature, 491(7426), 744–747, doi:10.1038/nature11593, 2012.

Gu, F., Zonneveld, K. A. F., Chiessi, C. M., Arz, H. W., Pätzold, J. and Behling, H.: Long-term vegetation, climate and ocean dynamics

inferred from a 73,500 years old marine sediment core (GeoB2107-3) off southern Brazil, Quat. Sci. Rev., 172, 55–71, doi:https://doi.org/10.1016/j.quascirev.2017.06.028, 2017.

Gu, F., Chiessi, C. M., Zonneveld, K. A. F. and Behling, H.: Late Quaternary environmental dynamics inferred from marine sediment core GeoB6211-2 off southern Brazil, Palaeogeogr. Palaeoclimatol. Palaeoecol., 496, 48–61, doi:https://doi.org/10.1016/j.palaeo.2018.01.015, 2018.

Gu, F., Pätzold, J. and Behling, H.: Evidence of cooling in the tropical South Atlantic off southeastern Brazil during the last 50 kyr, Rev. Palaeobot. Palynol., 104128, doi:10.1016/j.revpalbo.2019.104128, 2019.

Howe, J. N. W., Huang, K.-F., Oppo, D. W., Chiessi, C. M., Mulitza, S., Blusztajn, J. and Piotrowski, A. M.: Similar mid-depth Atlantic water mass provenance during the Last Glacial Maximum and Heinrich Stadial 1, Earth Planet. Sci. Lett., 490, 51–61, doi:https://doi.org/10.1016/j.epsl.2018.03.006, 2018.

Jaeschke, A., Rühlemann, C., Arz, H., Heil, G. and Lohmann, G.: Coupling of millennial-scale changes in sea surface temperature and precipitation off northeastern Brazil with high-latitude climate shifts during the last glacial period, Paleoceanography, 22(4), 1–10, doi:10.1029/2006PA001391, 2007.

Jennerjahn, T. C., Ittekkot, V., Arz, H. W., Behling, H., Pätzold, J. and Wefer, G.: Asynchronous terrestrial and marine signals of climate change during Heinrich events., Science, 306(5705), 2236–2239, doi:10.1126/science.1102490, 2004.

Lamy, F., Kaiser, J., Arz, H. W., Hebbeln, D., Ninnemann, U., Timm, O., Timmermann, A. and Toggweiler, J. R.: Modulation of the bipolar seesaw in the Southeast Pacific during Termination 1, Earth Planet. Sci. Lett., 259(3–4), 400–413, doi:10.1016/j.epsl.2007.04.040, 2007.

Lessa, D. V. O., Venancio, I. M., dos Santos, T. P., Belem, A. L., Turcq, B. J., Sifeddine, A. and Albuquerque, A. L. S.: Holocene oscillations of Southwest Atlantic shelf circulation based on planktonic foraminifera from an upwelling system (off Cabo Frio, Southeastern Brazil), Holocene, 26(8), doi:10.1177/0959683616638433, 2016.

Lessa, D. V. O., Santos, T. P., Venancio, I. M. and Albuquerque, A. L. S.: Offshore expansion of the Brazilian coastal upwelling zones during Marine Isotope Stage 5, Glob. Planet. Change, 158(August), 13–20, doi:10.1016/j.gloplacha.2017.09.006, 2017.

Lessa, D. V. O., Santos, T. P., Venancio, I. M., Santarosa, A. C. A., dos Santos Junior, E. C., Toledo, F. A. L., Costa, K. B. and Albuquerque, A. L. S.: Eccentricity-induced expansions of Brazilian coastal upwelling zones, Glob. Planet. Change, 179(May), 33–42, doi:10.1016/j.gloplacha.2019.05.002, 2019.

Li, M., Hinnov, L. and Kump, L.: Acycle: Time-series analysis software for paleoclimate research and education, Comput. Geosci., 127(September 2018), 12–22, doi:10.1016/j.cageo.2019.02.011, 2019.

Lisiecki, L. E. and Raymo, M. E.: A Pliocene-Pleistocene stack of 57 globally distributed benthic δ 18O records, Paleoceanography, 20(1), 1–17, doi:10.1029/2004PA00107110.1029/2003PA000942; Andersson, C., Wamke, D.A., Channell, J.E.T., Stoner, J., Jansen, E., The mid-Pliocene (4.2-2.6 Ma) benthic stable isotope record of the Southern Ocean: ODP Sites 1092 and 704, Meteor Rise (2002) Palaeogeogr. Palaeoclimatol. Palaeoecol., 182, pp. 165-181; Bard, E., Hamelin, B., Fairbanks, R.G., U-Th ages obtained by mass spectrometry in corals from Barbados: Sea level during the past 130,000 years (1990) Nature, 346, pp. 456-458; Bassinot, F.C., Labeyri, 2005.

Liu, W., Xie, S.-P., Liu, Z. and Zhu, J.: Overlooked possibility of a collapsed Atlantic Meridional Overturning Circulation in warming climate, Sci. Adv., 3(1), e1601666, doi:10.1126/sciadv.1601666, 2017.

Locarnini, R. A., Mishonov, A. V, Antonov, J. I., Boyer, T. P., Garcia, H. E., Baranova, O. K., Zweng, M. M., Paver, C. R., Reagan, J. R., Johnson, D. R., Hamilton, M., Seidov, D. and Technical: World Ocean Atlas 2013, edited by S. Levitus and M. A., NOAA Atlas NESDIS 73., 2013.

Lund, D. C., Tessin, A. C., Hoffman, J. L. and Schmittner, A.: Southwest Atlantic water mass evolution during the last deglaciation,

Paleoceanography, 30(5), 477–494, doi:10.1002/2014PA002657, 2015.

Lüthi, D., Le Floch, M., Bereiter, B., Blunier, T., Barnola, J.-M., Siegenthaler, U., Raynaud, D., Jouzel, J., Fischer, H., Kawamura, K. and Stocker, T. F.: High-resolution carbon dioxide concentration record 650,000–800,000 years before present, Nature, 453(7193), 379–382,
420   doi:10.1038/nature06949, 2008.

Mendonça, L. F., Souza, R. B., Aseff, C. R. C., Pezzi, L. P., Möller, O. O. and Alves, R. C. M.: Regional modeling of the water masses and circulation annual variability at the Southern Brazilian Continental Shelf, J. Geophys. Res. Ocean., 122(2), 1232–1253, doi:10.1002/2016JC011780, 2017.

Möller, O. O., Piola, A. R., Freitas, A. C. and Campos, E. J. D.: The effects of river discharge and seasonal winds on the shelf off southeastern
425   South America, Cont. Shelf Res., 28(13), 1607–1624, doi:10.1016/j.csr.2008.03.012, 2008.

Mulitza, S. and al, et: Temperature surface relationships of planktonic foraminifera collected from surface waters., Paleogeography, Palaeoclimatol. Palaecology, 202(1), 143–152, 2003.

Mulitza, S., Chiessi, C. M., Schefuß, E., Lippold, J., Wichmann, D., Antz, B., Mackensen, A., Paul, A., Prange, M., Rehfeld, K., Werner, M., Bickert, T., Frank, N., Kuhnert, H., Lynch-Stieglitz, J., Portilho-Ramos, R. C., Sawakuchi, A. O., Schulz, M., Schwenk, T., Tiedemann,
430   R., Vahlenkamp, M. and Zhang, Y.: Synchronous and proportional deglacial changes in Atlantic meridional overturning and northeast Brazilian precipitation, Paleoceanography, 32(6), 622–633, doi:10.1002/2017PA003084, 2017.

Müller, P. J., Kirst, G., Ruhland, G., von Storch, I. and Rosell-Melé, A.: Calibration of the alkenone paleotemperature index U37K′ based on core-tops from the eastern South Atlantic and the global ocean (60°N-60°S), Geochim. Cosmochim. Acta, 62(10), 1757–1772, doi:https://doi.org/10.1016/S0016-7037(98)00097-0, 1998.

435   Nagai, R. H., Ferreira, P. A. L., Mulkherjee, S., Martins, M. V, Figueira, R. C. L., Sousa, S. H. M. and Mahiques, M. M.: Hydrodynamic controls on the distribution of surface sediments from the southeast South American continental shelf between 23°S and 38°S, Cont. Shelf Res., 89, 51–60, doi:https://doi.org/10.1016/j.csr.2013.09.016, 2014.

Novello, V. F., Cruz, F. W., Vuille, M., Stríkis, N. M., Edwards, R. L., Cheng, H., Emerick, S., de Paula, M. S., Li, X., Barreto, E. de S., Karmann, I. and Santos, R. V: A high-resolution history of the South American Monsoon from Last Glacial Maximum to the Holocene,
440   Sci. Rep., 7, 44267, doi:10.1038/srep44267https://www.nature.com/articles/srep44267#supplementary-information, 2017.

Olson, D. B., Podestá, G. P., Evans, R. H. and Brown, O. B.: Temporal variations in the separation of Brazil and Malvinas Currents, Deep Sea Res. Part A. Oceanogr. Res. Pap., 35(12), 1971–1990, doi:10.1016/0198-0149(88)90120-3, 1988.

Oppo, D. W., Curry, W. B. and Mcmanus, J. F.: What do benthic 13C and 18O data tell us about Atlantic circulation during Heinrich Stadial 1?, , 353–368, doi:10.1002/2014PA002667.Received, 2015.

445   Palma, E. D., Matano, R. P. and Piola, A. R.: A numerical study of the Southwestern Atlantic Shelf circulation: Stratified ocean response to local and offshore forcing, J. Geophys. Res. Ocean., 113(11), 1–22, doi:10.1029/2007JC004720, 2008.

Peterson, R. G. and Stramma, L.: Upper-level circulation in the South Atlantic Ocean, Prog. Oceanogr., 26(1), 1–73, doi:https://doi.org/10.1016/0079-6611(91)90006-8, 1991.

Pezzi, L. P., Souza, R. B., Farias, P. C., Acevedo, O. and Miller, A. J.: Air-sea interaction at the Southern Brazilian Continental Shelf: In
450   situ observations, J. Geophys. Res. Ocean., 121(9), 6671–6695, doi:10.1002/2016JC011774, 2016.

Piola, A. R., Campos, E. J. D., Möller, O. O., Charo, M. and Martinez, C.: Subtropical Shelf Front off eastern South America, J. Geophys. Res. Ocean., 105(C3), 6565–6578, doi:10.1029/1999JC000300, 2000.

Piola, A. R., Matano, R. P., Palma, E. D., Möller, O. O. and Campos, E. J. D.: The influence of the Plata River discharge on the western South Atlantic shelf, Geophys. Res. Lett., 32(1), 1–4, doi:10.1029/2004GL021638, 2005.

455   Piola, A. R., Möller, O. O., Guerrero, R. A. and Campos, E. J. D.: Variability of the subtropical shelf front off eastern South America: Winter 2003 and summer 2004, Cont. Shelf Res., 28(13), 1639–1648, doi:https://doi.org/10.1016/j.csr.2008.03.013, 2008.

Portilho-Ramos, R. da C., Ferreira, F., Calado, L., Frontalini, F. and de Toledo, M. B.: Variability of the upwelling system in the southeastern Brazilian margin for the last 110,000years, Glob. Planet. Change, 135, 179–189, doi:https://doi.org/10.1016/j.gloplacha.2015.11.003, 2015.

460   Portilho-Ramos, R. da C., Pinho, T. M. L., Chiessi, C. M. and Barbosa, C. F.: Understanding the mechanisms behind high glacial productivity in the southern Brazilian margin, Clim. Past, 15(3), 943–955, doi:10.5194/cp-15-943-2019, 2019.

Prahl, F. G. and Wakeham, S. G.: Calibration of unsaturation patterns in long-chain ketone compositions for palaeotemperature assessment, Nature, 330(6146), 367–369 [online] Available from: http://dx.doi.org/10.1038/330367a0, 1987.

Reimer, P. J., Bard, E., Bayliss, A., Beck, J. W., Blackwell, P. G. and Ramsey, C. B.: IntCal13 and Marine13 Radiocarbon Age Calibration

465   Curves 0–50,000 Years cal BP, Radiocarbon, 55(4), 1869–1887, doi:10.2458/azu_js_rc.55.16947, 2013.

Rühlemann, C., Mulitza, S., Müller, P. J., Wefer, G. and Zahn, R.: Warming of the tropical Atlantic Ocean and slowdown of thermohaline circulation during the last deglaciation, Nature, 402(6761), 511–514, doi:10.1038/990069, 1999.

Santos, T. P., Lessa, D. O., Venancio, I. M., Chiessi, C. M., Mulitza, S., Kuhnert, H., Govin, A., Machado, T., Costa, K. B., Toledo, F., Dias, B. B. and Albuquerque, A. L. S.: Prolonged warming of the Brazil Current precedes deglaciations, Earth Planet. Sci. Lett., 463, 1–12,

470   doi:https://doi.org/10.1016/j.epsl.2017.01.014, 2017a.

Santos, T. P., Lessa, D. O., Venancio, I. M. and Chiessi, C. M.: The impact of the AMOC resumption in the western South Atlantic thermocline at the onset of the Last Interglacial, , 1–8, doi:10.1002/2017GL074457, 2017b.

de Souza, R. B. and Robinson, I. S.: Lagrangian and satellite observations of the Brazilian Coastal Current, Cont. Shelf Res., 24(2), 241–262, doi:10.1016/j.csr.2003.10.001, 2004.

475   Stevenson, M. R., Dias-Brito, D., Stech, J. L. and Kampel, M.: How do cold water biota arrive in a tropical bay near Rio de Janeiro, Brazil?, Cont. Shelf Res., 18(13), 1595–1612, doi:10.1016/S0278-4343(98)00029-6, 1998.

Stramma, L. and England, M.: On the water masses and mean circulation of the South Atlantic Ocean, J. Geophys. Res. Ocean., 104(C9), 20863–20883, doi:10.1029/1999JC900139, 1999.

Stríkis, N. M., Chiessi, C. M., Cruz, F. W., Vuille, M., Cheng, H., de Souza Barreto, E. A., Mollenhauer, G., Kasten, S., Karmann, I.,

480   Edwards, R. L., Bernal, J. P. and Sales, H. dos R.: Timing and structure of Mega-SACZ events during Heinrich Stadial 1, Geophys. Res. Lett., 42(13), 5477-5484A, doi:doi:10.1002/2015GL064048, 2015.

Stríkis, N. M., Cruz, F. W., Barreto, E. A. S., Naughton, F., Vuille, M., Cheng, H., Voelker, A. H. L., Zhang, H., Karmann, I., Edwards, R. L., Auler, A. S., Santos, R. V. and Sales, H. R.: South American monsoon response to iceberg discharge in the North Atlantic., Proc. Natl. Acad. Sci. U. S. A., 201717784, doi:10.1073/pnas.1717784115, 2018.

485   Synal, H.-A., Stocker, M. and Suter, M.: MICADAS: A new compact radiocarbon AMS system, Nucl. Instruments Methods Phys. Res. Sect. B Beam Interact. with Mater. Atoms, 259(1), 7–13, doi:https://doi.org/10.1016/j.nimb.2007.01.138, 2007.

Tessin, A. C. and Lund, D. C.: Isotopically depleted carbon in the mid-depth South Atlantic during the last deglaciation, Paleoceanography, 28(2), 296–306, doi:10.1002/palo.20026, 2013.

Venancio, I. M., Mulitza, S., Govin, A., Santos, T. P., Lessa, D. O., Albuquerque, A. L. S., Chiessi, C. M., Tiedemann, R., Vahlenkamp, M.,

490   Bickert, T. and Schulz, M.: Millennial- to orbital-scale responses of western equatorial Atlantic thermocline depth to changes in the trade wind system since the Last Interglacial, Paleoceanogr. Paleoclimatology, 0(ja), doi:doi:10.1029/2018PA003437, 2018.

Veres, D., Bazin, L., Landais, A., Toyé Mahamadou Kele, H., Lemieux-Dudon, B., Parrenin, F., Martinerie, P., Blayo, E., Blunier, T.,

Capron, E., Chappellaz, J., Rasmussen, S. O., Severi, M., Svensson, A., Vinther, B. and Wolff, E. W.: The Antarctic ice core chronology (AICC2012): an optimized multi-parameter and multi-site dating approach for the last 120 thousand years, Clim. Past, 9(4), 1733–1748,
495   doi:10.5194/cp-9-1733-2013, 2013.

Waelbroeck, C., Paul, a., Kucera, M., Rosell-Melé, a., Weinelt, M., Schneider, R., Mix, a. C., Abelmann, a., Armand, L., Bard, E., Barker, S., Barrows, T. T., Benway, H., Cacho, I., Chen, M.-T., Cortijo, E., Crosta, X., de Vernal, a., Dokken, T., Duprat, J., Elderfield, H., Eynaud, F., Gersonde, R., Hayes, a., Henry, M., Hillaire-Marcel, C., Huang, C.-C., Jansen, E., Juggins, S., Kallel, N., Kiefer, T., Kienast, M., Labeyrie, L., Leclaire, H., Londeix, L., Mangin, S., Matthiessen, J., Marret, F., Meland, M., Morey, a. E., Mulitza, S., Pflaumann, U.,
500   Pisias, N. G., Radi, T., Rochon, a., Rohling, E. J., Sbaffi, L., Schäfer-Neth, C., Solignac, S., Spero, H., Tachikawa, K. and Turon, J.-L.: Constraints on the magnitude and patterns of ocean cooling at the Last Glacial Maximum, Nat. Geosci., 2(2), 127–132, doi:10.1038/ngeo411, 2009.

Zhang, Y., Chiessi, C. M., Mulitza, S., Zabel, M., Trindade, R. I. F., Hollanda, M. H. B. M., Dantas, E. L., Govin, A., Tiedemann, R. and Wefer, G.: Origin of increased terrigenous supply to the NE South American continental margin during Heinrich Stadial 1 and the Younger
505   Dryas, Earth Planet. Sci. Lett., 432, 493–500, doi:10.1016/j.epsl.2015.09.054, 2015.

Zhang, Y., Chiessi, C. M., Mulitza, S., Sawakuchi, A. O., Häggi, C., Zabel, M., Portilho-Ramos, R. C., Schefuß, E., Crivellari, S. and Wefer, G.: Different precipitation patterns across tropical South America during Heinrich and Dansgaard-Oeschger stadials, Quat. Sci. Rev., 177, 1–9, doi:https://doi.org/10.1016/j.quascirev.2017.10.012, 2017.

510
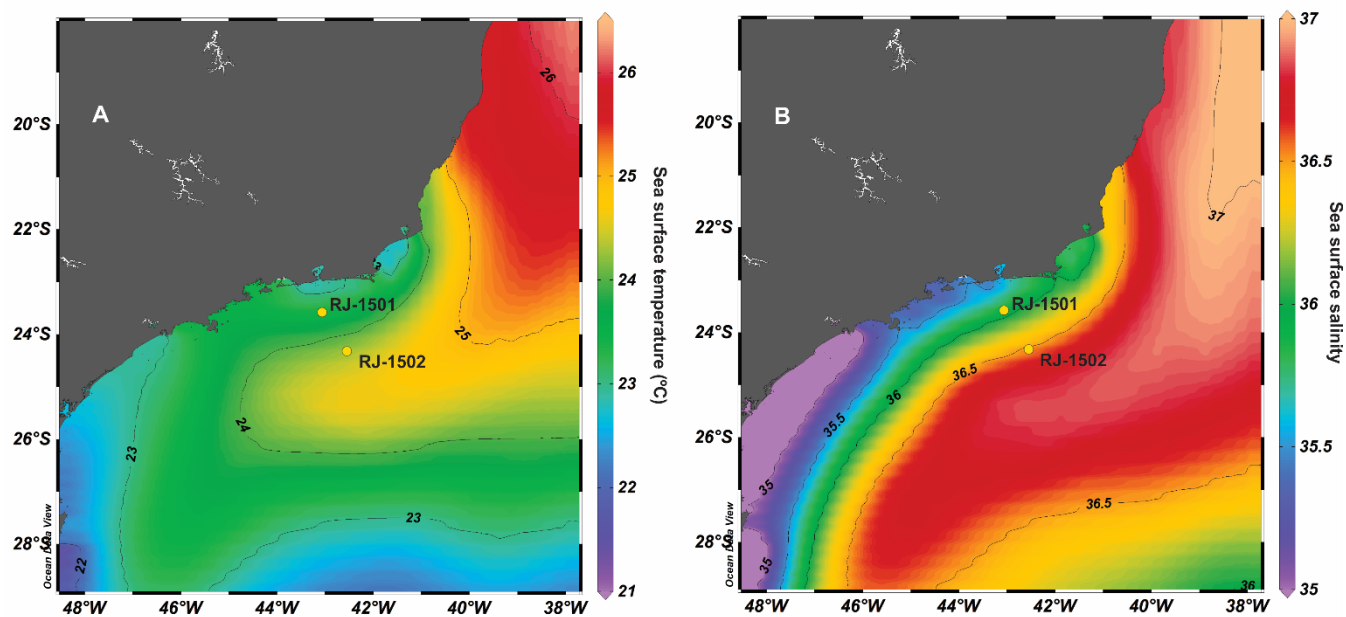
515

Figure 1 – Position of the marine sediment cores RJ-1501 (23°58'14.3"S/43°06'35.1"W; 328 m water depth) and RJ-1502 (24°32'57.6" S/42°55'42.9"W; 1598 m water depth), in the upper and lower continental slope of the subtropical western South Atlantic, respectively. The maps feature the annual sea surface temperature (A) and sea surface salinity (B). Temperature and salinity grids are derived from the World Ocean Atlas 2013 (Locarnini et al., 2013; Zweng et al., 2013). This figure was

520   produced using the Ocean Data View software (Schlitzer, 2017).
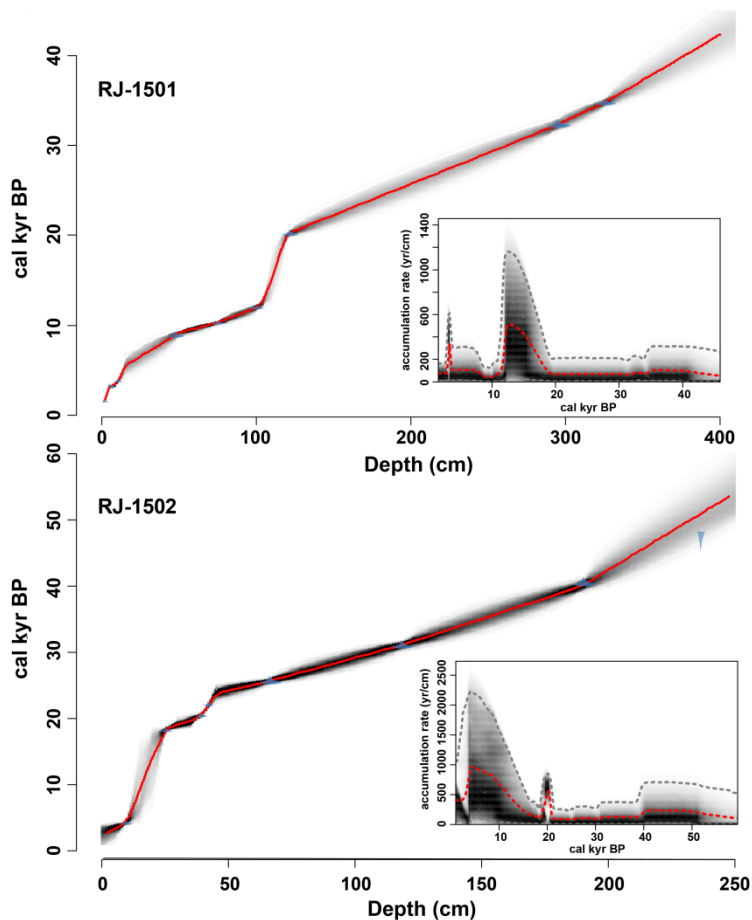
Figure 2 – Bayesian age-depth model and sediment accumulation rate (years/cm) for cores RJ-1501 (upper panel) and RJ-1502 (lower panel). The ^{14}C ages were calibrated by the curve IntCal13 (Reimer et al., 2013) and modeled with a reservoir age of 375 ± 36 years from ten local records. Thick (larger panels) and dashed (smaller panels) red lines depict the highest probalistic model for the ages and accumulation rate, respectively. Dashed (smaller panels) grey lines indicated the upper and bottom limits of the accumulation rate.
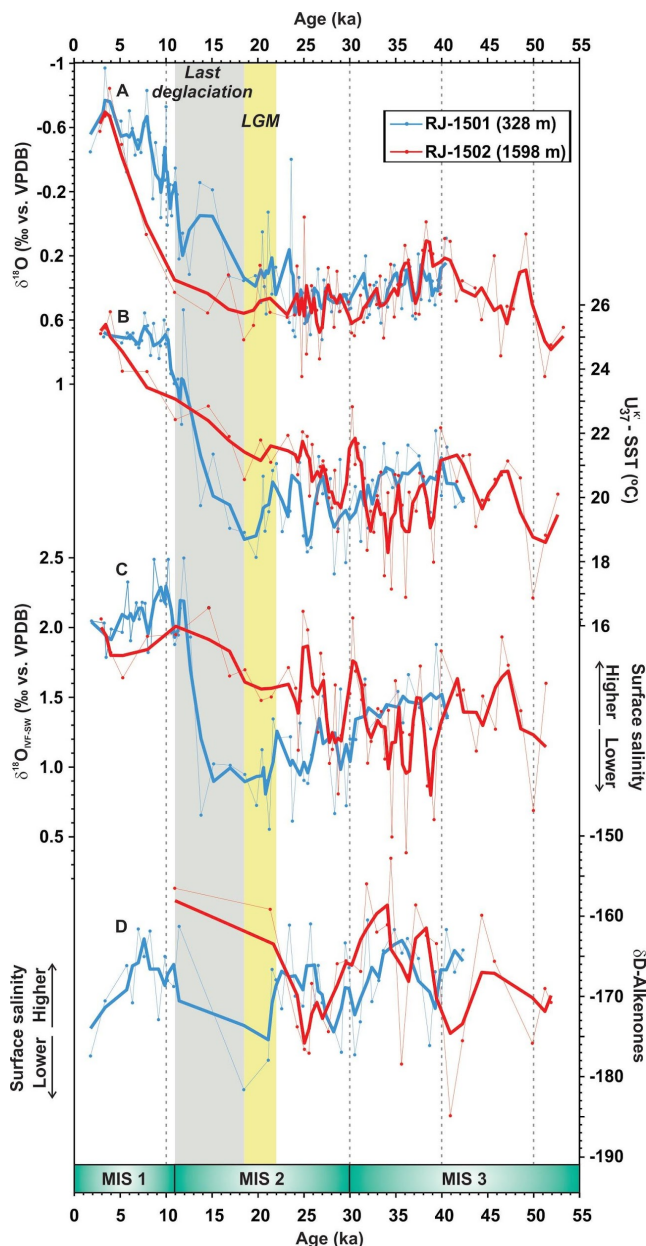
Figure 3 – Organic and inorganic proxies developed from marine sediment cores RJ-1501 (blue) and RJ-1502 (red). A: oxygen isotope ($\delta^{18}O$) of the planktic foraminifera *Globigerinoides ruber* (white). B: Alkenone ($U_{37}^{K'}$)-derived sea surface temperature
530 (SST). C: Ice-volume free sea water oxygen isotope ($\delta^{18}O_{IVF-SW}$) derived from the $\delta^{18}O$ composition of *G. ruber* and $U_{37}^{K'}$-derived SST. D: δD-Alkenones. Records are depicted by the original data (dots and thin line) and the respective three-point running average (thick line). Marine Isotope Stages (MIS) are indicated at the bottom of the panel.

535
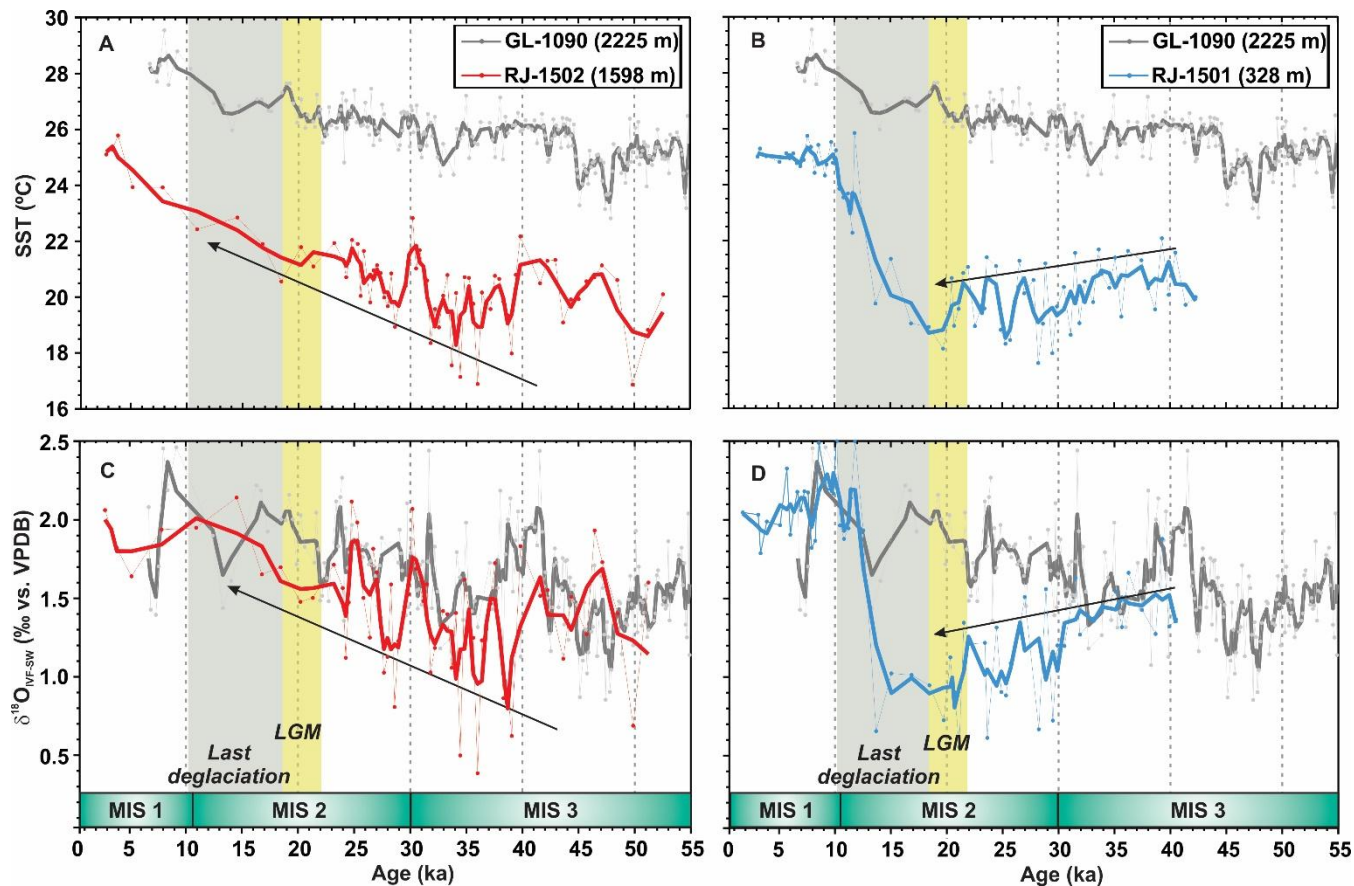
Figure 4 – Comparison of the records from marine sediment cores RJ-1501 (blue), RJ-1502 (red) (this study) and GL-1090 (grey) (Santos et al., 2017a). A and B: Alkenone ($U_{37}^{K'}$)-derived sea surface temperature (SST) from cores RJ-1502 and RJ-1501 and Mg/Ca-derived SST from core GL-1090. C and D: Ice-volume free sea water oxygen isotope ($\delta^{18}O_{\text{IVF-SW}}$) from cores RJ-1502, RJ-1501 and GL-1090. Records are depicted by the original data (dots and thin line) and the respective three-point running average (thick line). Yellow and grey bars denote the Last Glacial Maximum (LGM) and last deglaciation, respectively. Marine Isotope Stages (MIS) are indicated at the bottom of the panel.
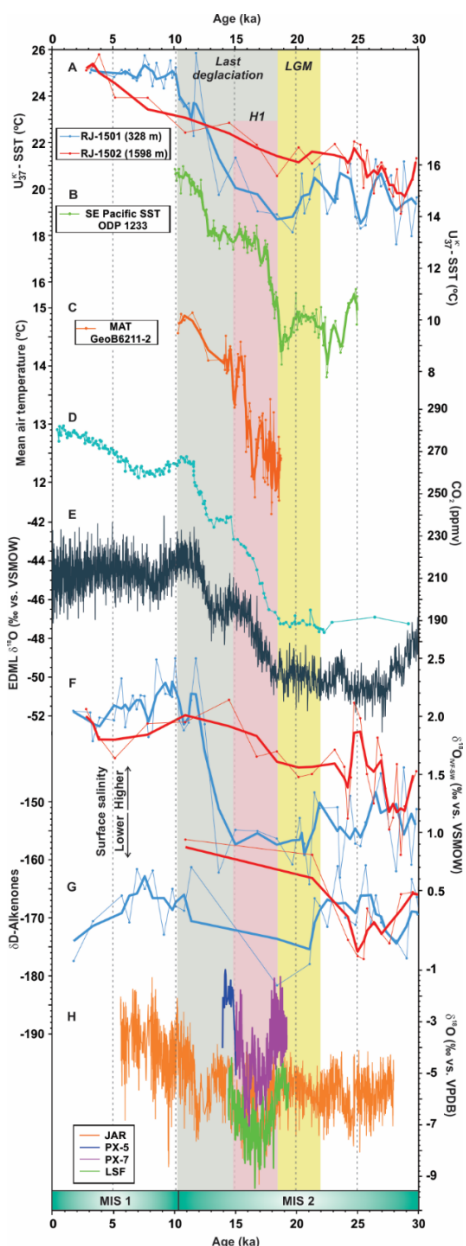
545 Figure 5 – Comparison of the marine sediment cores RJ-1501 (blue) and RJ-1502 (red) with other Southern Hemisphere records. A: Alkenone ($U_{37}^{K'}$)-derived sea surface temperature (SST) from cores RJ-1502 and RJ-1501. B: $U_{37}^{K'}$-derived SST from ODP Site 1233 (Lamy et al., 2007). C: Mean air temperature from GeoB6211-2 (Chiessi et al., 2015). D: Carbon dioxide (CO_2) concentration from Antarctic EPICA Dome C (Lüthi et al., 2008) on the Antarctic Ice Core Chronology (AICC2012) (Veres et al., 2013; Bazin et al., 2013). E: Antarctic oxygen isotope from EDML (EPICA, 2004) on the AICC2012 chronology. F:
550 Ice-volume free sea water oxygen isotope ($\delta^{18}O_{IVF-SW}$) from RJ-1501 and RJ-1502. G: δD-Alkenones from RJ-1501 and RJ-1502. H: Speleothem oxygen isotope from Jaraguá cave (JAR) (Novello et al., 2017) and Paixão (PX-5 and PX-7) and Lapa sem Fim (LSF) caves (Stríkis et al., 2015). Records are depicted by the original data (dots and thin line) and the respective three-point running average (thick line). Yellow, red and grey bars denote the Last Glacial Maximum (LGM), Heinrich stadial 1 and last deglaciation, respectively Marine Isotope Stages (MIS) are indicated at the bottom of the panel.

555

560
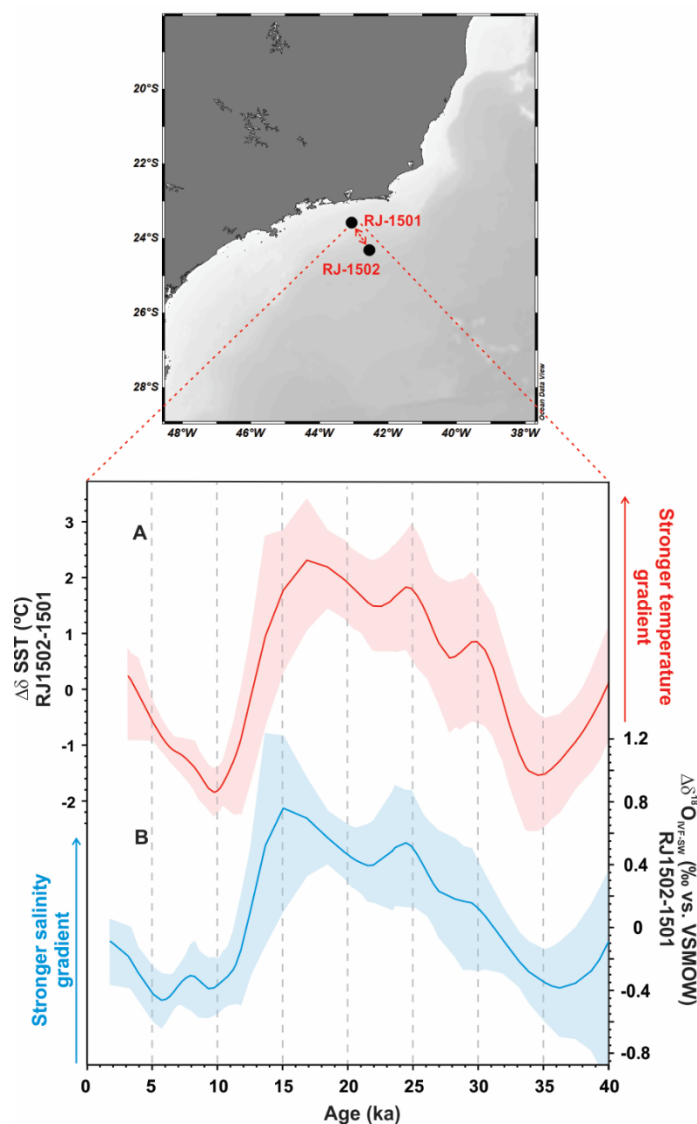
Figure 6 – Sea surface temperature and salinity gradient formed in the area between the marine sediment cores RJ-1501 and RJ-1502 (map in the uppermost panel) during the Last Glacial Maximum and early-deglaciation interval. Records were placed on a common time-scale (RJ-1501) and the mean around zero were subtracted (RJ-1502 minus RJ-1501) to produce ΔAlkenone ($U^{K'}_{37}$)-derived sea surface temperature (SST) and Δδ-ice-volume free sea water oxygen isotope ($\Delta\delta^{18}O_{IVF-SW}$). The records were bootstrapped using the Acycle software with a 10% window (Li et al., 2019) and presented with the 2.5[th] and 97.5[th] percentiles (red and blue shaded areas). A: $\Delta\delta U^{K'}_{37}$-derived SST. B: $\Delta\delta^{18}O_{IVF-SW}$.

570

Table 1. Accelerator mass spectrometer radiocarbon (MICADAS) dates and calibrated ages used for age-depth models of cores RJ-1501 and RJ-1502.

Station	Core Depth (cm)	ID-Lab*	Species	Radiocarbon Age (yrBP)	± 1s error	Calibrated Age (calyr BP)	Min-Max (calyr BP)
RJ-1501	2	82195	*G. ruber, G. sacculifer*	2168	65	1756	1574-1930
	5	84479	*G. ruber, G. sacculifer*	3647	118	3138	2861-3397
	8	82194	*G. ruber, G. sacculifer*	3367	68	3361	3202-3558
	11	84478	*G. ruber, G. sacculifer*	4078	66	3904	3706-4094
	50	85107	*G. ruber, G. sacculifer*	8649	141	9145	8705-9496
	74	82193	*G. ruber, G. sacculifer*	9426	84	10273	9984-10533
	101	84477	*G. ruber, G. sacculifer*	10614	83	12090	11691-12453
	119	82192	*G. ruber, G. sacculifer*	17050	126	19706	19039-20272
	290	82191	*G. ruber, G. sacculifer*	28270	282	31955	31244-32779
	323	84476	*G. ruber, G. sacculifer*	30927	280	34585	34048-35143
RJ-1502	8	84509	*G. ruber, G. sacculifer*	4055	86	3841	3353-4239
	26	85049	*G. ruber, G. sacculifer*	15418	111	18454	18123-18793
	38	85048	*G. ruber, G. sacculifer*	16813	117	20236	19903-20614
	41	85047	*G. ruber, G. sacculifer*	18392	129	21321	20966-21676
	65	84510	*G. ruber, G. sacculifer*	21259	153	25523	24939-25966
	116	85106	*G. ruber, G. sacculifer*	26638	347	30784	29916-31447
	185	84508	*G. ruber, G. sacculifer*	34791	413	39395	38087-40532
	245	84507	*G. ruber, G. sacculifer*	49358	597	52887	48659-58741

*Laboratory of Ion Beam Physics (ETH Zurich).